Polymer reinforced by flax fibres as a viscoelastoplastic material

C. Poilâne[a,b,c,d,e,*], Z. E. Cherif[a,b,c,d,e], F. Richard[f,g], A. Vivet[a,b,c,d,e], B. Ben Doudou[a,b,c,d,e], J. Chen[a,b,c,d,e]

[a]Normandie Univ, France
[b]UNICAEN, CIMAP, F-14050 Caen, FRANCE
[c]ENSICAEN, F-14050 Caen, FRANCE
[d]CNRS, UMR 6252, F-14050 Caen, FRANCE
[e]CEA, UMR 6252, F-14050 Caen, FRANCE
[f]Université de Franche-Comté, FEMTO ST, F-25044 Besançon, FRANCE
[g]CNRS, UMR 6174, F-25044 Besançon, FRANCE

Abstract

Flax fibre reinforced polymers are at the heart of current scientific and societal concerns. However their mechanical behaviour is still poorly known despite significant scientific efforts, in particular the non-linear behaviour observed under tensile tests. In this paper, results of hardening, creep and repeated progressive tests under uniaxial loading performed on various quasi-unidirectional flax fibre reinforced composites are analyzed in terms of the volume fraction of fibre, the titration of yarn reinforcement and temperature testing. To identify the respective parts of pure elastic, viscoelastic and viscoplastic components in the global mechanical response, a phenomenological model is built based on seven independent parameters. The parameter identification based on experimental data and checked by a sensitivity analysis shows that the viscoelastic effects are non-significant at room temperature. The non-linear behaviour can mainly be attributed to viscoplastic effects. Viscoplastic modeling is based on a combination of two hardenings; the first classical (linear) one describes the translation of the elastic domain; the second (nonlinear) one describes a translation coupled with a contraction of the elastic domain during loading that improves the unloading behaviour during repeated progressive loading test.

Keywords: A. Flax/epoxy, A. Unidirectional composite, B. Viscoelastoplasticity, C. Phenomenological modelling, C. Identifiability analysis

*Corresponding author
Email address: `christophe.poilane@unicaen.fr` (C. Poilâne)

1. Introduction

Nowadays the composite sector is looking for ecological resources which will allow the replacement of synthetic fibres. The fibres usually utilised in composite materials have mineral or petrochemical origins such as glass, carbon and organic fibres. The economic stakes are high enough to justify their replacement; the management of the structures at the end-of-life cycle [1, 2], the increasing cost of fossil resources, and their disappearance in a near future, reinforce the investigations towards the use of natural fibres in composite industry [3, 4, 5, 6]. Flax (Linum usitatissimum Linaceae) fibre is a vegetal fibre. France is the first long flax fibre producer in the world, with the Normandy region as the national leader. The traditional market is the textile sector. Following the disruption of the European textile industry in recent years, the flax sector is seeking new opportunities. Therefore, reinforcement of composites by natural fibres will represent an important market for the flax sector. The particular properties of flax fibre reinforced polymers (FFRP) for both economic and environmental benefit are within the worldwide trend towards a sustainable development.

The performance of composite materials containing natural fibres has been studied for several decades [6]. The FFRP has often been compared to glass fibre reinforced polymers (GFRP) [7, 8, 9, 10]. This comparison originates from the specific properties of individual flax fibre which are of the same level as those of E-glass fibre [11, 12, 13]. The density of FFRP is lower (about 1.4 for FFRP against 1.8 for GFRP for a fibre percentage of $50\,\%$). However there are many differences between the FFRP and the GFRP. Flax fibres are not strictly included in the category of long fibre-reinforced materials. Indeed, individual flax fibre length varies from $4\,\mathrm{mm}$ to $80\,\mathrm{mm}$ for a diameter from $7\,\mathrm{\mu m}$ to $77\,\mathrm{\mu m}$ [14]. Furthermore, the compatibility between the fibre and the matrix is quite difficult to obtain. Despite extensive research aimed at overcoming this problem for decades [15, 16, 17, 18], the interface between fibre and matrix is not so good in the case of FFRP. These two behaviours (fibre length and fibre/matrix compability) explain the weak property of failure of FFRP compared to that of GFRP [19]. Moisture behaviour is also different. The water saturation of FFRP can reach $13.5\,\%$ in contrast to $1.05\,\%$ for a comparable GFRP [9]. High hydrophily of the flax fibre and porosity of the composite mainly due to imperfect interfaces

explain this phenomenon [18].

In this paper, we focus the discussion on another major difference between FFRP and GFRP: the presence of a yield point at room temperature. Indeed, the tensile behaviour of reinforced polymer by flax fibres shows two regions. This is visible on experimental curves in articles that do not deal only with unidirectional reinforcement [20, 21] but also with reinforcement by random mat of flax [22] or by other vegetable fibres [23, 24]. In order to achieve our goal, consolidation of flax/epoxy containing a different fibre-to-matrix ratio was performed by hot platen press and the mechanical properties have been characterised by tensile tests. We worked out, elaborated and tested four laminated composites from two categories of prepreg intended for unidirectional reinforcement (section 2). All the plates are elaborated with $0\deg$ oriented plies. Then we proceeded to the optimisation of the material that was intended to thin down prepreg by decreasing the titration of the yarns. The obtained results allow us to compare the performance of the products versus the fibre percentage, the titration of used yarns and the temperature (section 3). Finally, in the context of thermodynamics with internal variables [25], we developed a viscoelastoplastic model based on a previous phenomenological model [26] in order to explain the mechanical behaviour of flax/epoxy composite. We used repetitive progressive loading, creep and relaxation tests to identify and validate the model. Flax/epoxy behaviour is well described by a viscoelastic model in the first region and a viscoelastoplastic model in the second region (section 4).

2. Materials and methods

2.1. General characteristics of utilised fibres

The utilised fibres in the processing of tested prepreg are not subject to any particular selection. It should be noted that some studies have shown the utility, for the composite industry, of selecting flax varieties and preserving only the central part of the plant [27, 28]. This approach, that some manufacturers try to put into practice, has not been used here. Indeed, the objective of the prepreg is to penetrate the composite market without deeply modifying the working tools of flax professionals.

The preparation of flax fibres is thus carried out according to the four usual stages [29]: retting, scutching, heckling, and folding/drawing. Retting is a natural process carried out in Normandy by

the climate. After ripping out, the stems of the plant are left on the ground, in the form of swathes, in order to facilitate the action of natural micro-organisms. Degradation of pectin cements, supported by the alternation of heat and moisture, makes it possible to obtain the first separation of fibres and wood. Scutching consists in extracting fibres contained in the stems by rippling and picking the straws. The mechanical actions carried out on fibres include sorting, picking, rippling between two rib rollers, drawing by differential rolling and drafting. Heckling consists in carding the bundle of fibres in a succession of increasingly fine heckles (sort of comb). Folding/drawing of the flax allows to conglomerate fibres in order to obtain a several-meter long ribbon exploitable by the flax spinning mills. The ribbon's quality is standardised by mixture of fibres from different origins.

In the domain of vegetable fibres, flax fibres offer top-of-the-range performances [30]. We often divide the properties of fibres depending on their density in order to compare flax and conventional fibres (table 1). ρ is the mass density, E is the Young's modulus, σ_u is the ultimate stress (or failure stress), ε_u is the ultimate strain (or failure strain), E/ρ is the specific Young's modulus and σ_u/ρ is the specific ultimate stress. Owing to the origin of the tested product, the median values found in the literature [31] were selected and not those of the most performing flax fibres. As can be seen, the specific modulus of flax fibre is similar to that of E-glass fibre.

[Table 1 about here.]

2.2. Development of the yarns

The flax ribbons are transformed into yarns by flax spinning mills. The ribbon undergoes successive torsions and stretching in order to obtain the desired yarn titration. Titration is expressed in tex, i.e. in gram per kilometre of yarn. The cohesion of the yarn is mainly achieved through adhesion between constitutive fibres [32]. The yarns used in the present work come from either wet spinning or semi-wet spinning. In wet spinning, the flax ribbon is leached in a specific bath during the spinning process. In semi-wet spinning, it is only water buffered.

2.3. Studied Prepreg

The prepreg is developed in two stages: the formation stage, possibly in fabric textures (linen fabric), and the impregnation stage. Between these two stages, the flax yarns undergo a drying

and a patented treatment [33] carried out by the manufacturer [34]. It has the double function of ensuring the effectiveness of the interface between the resin and fibres and limiting the water absorption of the fibres. The used resin is a standard epoxy for prepregs (Hunstman Araldite LY5150/Aradur 5021/Hardener XB 3471 [35]), having the following average properties in tensile test at room temperature: Young's modulus 3.57 ± 0.05 GPa, failure strain 2.5 ± 0.5 %, failure stress 73 ± 5 MPa (manufacturer's data).

We tested four models of prepreg intended for a unidirectional reinforcement (UD). The first two models, UD380 and UD200, are only made up of warp threads developed from a weaver's beam. The other two models, FUD180 and FUD115, are woven. They contain a small amount of weft threads making it possible to provide cohesion in the product and to facilitate its handling. The properties of the tested prepregs are shown in table 2. The initial percentage by weight of resin is between 50 % and 60 %. It is clear that the term unidirectional is not perfectly appropriate to the tested prepregs. This is mainly true in the case of the prepregs which have weft threads. However, the density of yarns according to the weft threads is low enough to allow us to compare prepregs in the principal orientation. The four prepregs conform to the evolution of the materials desired by the manufacturer. There has been a twofold improvement of the material: the reduction in the titration of the linen yarns in order to decrease the thickness of the products, and the contraction of the warp threads in order to preserve a high fibre percentage.

[Table 2 about here.]

2.4. Development of composite plates and specimens

In our flax/epoxy composite study, all plies have the same orientation (0 deg). The number of plies depends on the product (see tab. 3). The process of the development of the composite plates is carried out by using a male mould and female mould according to the following stages:

- cutting of folds of 110 mm $\times$ 200 mm according to the chosen orientation,

- waxing of the moulds,

- stacking of the folds in the male mould,

- putting adjusted metallic plates which allow us to choose the air gap in the mould,

- placing and tightening of the female mould by screw,

- curing in enclosure equipped with a thermostat in atmospheric pressure,

- removing the composite plate from the mould after return in room temperature.

The relationship between fold number and thickness of the plates allows us to slightly act on the volumic percentage of the fibres V^r. Consequently, the resin surplus is more or less important according to this ratio. Curing is in conformity with the manufacturer's instructions [35], $30\,\mathrm{min}$ at $80\,°\mathrm{C}$ and then $60\,\mathrm{min}$ at $130\,°\mathrm{C}$.

The specimens, $20\,\mathrm{mm} \times 200\,\mathrm{mm}$, are cut out with a diamond disc. Water cooling is utilised in order to avoid burning the composite. After drying, heels are stuck on the specimens in compliance with the ISO 527-4 and ISO 527-5 standards [36, 37].

2.5. Mass density of matrix and fibre

Mass densities of reinforcement ρ^r and matrix ρ^m have to be known in order to estimate mass density of composite material ρ^c. The matrix is composed of an epoxy resin, a hardener paste, and a hardener. The density of the matrix after polymerisation was measured using the normalised pycnometer method (ISO 1183-1 [38]). Nine samples were prepared with the same resin under the same conditions as those used to prepare composites. We obtain the mass density $\rho^m = 1204 \pm 10\,\mathrm{kg\,m^{-3}}$.

The density ρ^r of individual fibres of flax varies from $1380\,\mathrm{kg\,m^{-3}}$ to $1540\,\mathrm{kg\,m^{-3}}$ according to the literature [39, 40]. To prevent water absorption during measurements with a pycnometer we conducted a measurement by a direct method. A hundred and fifty individual fibres of different lengths were taken from a scutched flax ribbon. These fibres were separated randomly into a set of hundred fibres and a set of fifty fibres. The first set was used to measure the linear density of fibres per unit of dry flax. The length of each fibre was measured. The total length of fibres was $4.905\,\mathrm{m}$. This set was weighed with a Mettler Toledo®XS105 balance (accuracy $10^{-5}\,\mathrm{g}$). The moisture content of the flax fibres under ambient condition is $8\,\%$ (measured on fabrics before impregnation by the resin). After adjustment of 8%, the linear density of dried flax fibres is obtained: $\rho_L^r =$

$662 \pm 8\,\mu\mathrm{g\,m^{-1}}$. The second set was used to measure the middle section of individual fibre of flax. Each fibre was fixed in a paper frame. The transverse dimension t^r of each fibre was measured under a microscope all about $100\,\mu\mathrm{m}$. A mean value $\bar{t}^r = 23.3 \pm 7.3\,\mu\mathrm{m}$ was obtained. We assume that the representative section of the fibre is hexagonal and that $\bar{t}^r$ is the average diameter of the equivalent circular section. This leads to a flax density of $1549 \pm 18\ \mathrm{kg\,m^{-3}}$ without removing the section of the lumen (hollow section in the center of fibre). This density is consistent with the value $\rho^r = 1540\,\mathrm{kg\,m^{-3}}$ mentioned in the literature [39]. We retain this last value for fibre percentage computation of FFRP.

2.6. Mechanical tests

We performed tensile tests in the principal orientation (that of the warp threads). Loading was applied to the specimens using a hydraulic machine Instron® $100\,\mathrm{kN}$, at a cross-head speed of $2\,\mathrm{mm\,min^{-1}}$ (according to [36, 37]). An extensometer with a gauge length of $12.5\,\mathrm{mm}$ was attached to the specimen in order to measure the longitudinal strain. The testing consisted mainly of:

- monotonic tensile tests at atmospheric temperature,

- tensile tests at $20\,°\mathrm{C}$, $50\,°\mathrm{C}$, $100\,°\mathrm{C}$ and $150\,°\mathrm{C}$ in repetitive progressive loading.

Each monotonic test is carried out on a series of four or five specimens. The repetitive progressive loading instruction is described in figure 7(a). The results of a monotonic test must be known before launching a test of this type.

Two creep tests and a relaxation test were also carried out in order to identify and validate the parameters of the phenomenological model.

2.7. Mechanical behaviour model

In order to provide an accurate prediction of the uniaxial mechanic response of FFRP at $20\,°\mathrm{C}$, a viscoelastoplastic model has been developped. The total strain ε is partitioned in an elastic part ε^e (instantaneous reversible strain) and an inelastic part ε^{in} which is the sum of viscoelastic contribution ε^{ve} (time-dependent reversible strain) and viscoplastic contribution ε^{vp} (time-dependent

irreversible strain):

$$\varepsilon = \varepsilon^e + \varepsilon^{in} = \varepsilon^e + \varepsilon^{ve} + \varepsilon^{vp}. \tag{1}$$

In the context of thermodynamics with internal variables [25], the standardised framework [41] assumes that mechanical behaviour is obtained when two potentials are defined: a free energy density ψ to define state laws and a dissipation potential Ω to determine flow direction. Based on experimental results (section 2.6) and by implying that elasticity and inelastic behaviours are uncoupled, the two potentials are proposed.

The state laws can then be written as:

$$\sigma = \rho \frac{\partial \psi}{\partial \varepsilon^e} \tag{2}$$

$$X_i = \rho \frac{\partial \psi}{\partial \alpha_i} \tag{3}$$

where α_i and X_i variables represent inelastic phenomena, ρ is the mass density, and σ is the Cauchy's stress.

And the evolution of internal variables is expressed as:

$$\dot{\varepsilon}^{in} = \frac{\partial \Omega}{\partial \sigma} = \dot{\varepsilon}^{ve} + \dot{\varepsilon}^{vp} \tag{4}$$

$$\dot{\alpha}_i = -\frac{\partial \Omega}{\partial X_i}. \tag{5}$$

The system of ordinary differential equations has been solved with an homemade simulation software MIC2M [42] using an algorithm based on the Runge-Kutta method. The constitutive material parameters of the model have been identified using an inverse method which is presented in the next section.

2.8. Parametric identification and identifiability analysis

An inverse method approach is used to extract the constitutive parameters from the experimental strain measurements. This approach consists of an optimisation problem where the objective is to minimize the gap between the experimental results (section 2.6) and the numerical results (section 2.7):

$$\Theta^* = \underset{\Theta}{\operatorname{argmin}} f(\Theta) \tag{6}$$

where the vector $\boldsymbol{\Theta} = [\theta_1, \cdots, \theta_n]$ collects the unknown parameters to be identified and $f(\boldsymbol{\Theta})$ is the cost function, i.e. the gap between the experimental strain ε_m (m "measured") and the numerical results ε_c (c "calculated"), which can be defined for one experimental test as:

$$f(\boldsymbol{\Theta}) = \sum_{i=1}^{N} \left(\frac{\varepsilon_c(\boldsymbol{\Theta}, t_i) - \varepsilon_m(t_i)}{N \varepsilon_{\max}} \right)^2. \tag{7}$$

In equation (7), the ith data point corresponds to the acquisition time t_i. N is the number of the acquisition times in the experimental test. $\varepsilon_{\max}$ is a weighting coefficient defined as the maximum strain values in the considered test. If several tests are used, the data points are added to the cost function by the same principle of normalization.

The minimization problem (6 was solved using an algorithm based on the Levenberg-Marquardt method coupled with genetic approach implemented in MIC2M sofware [42].

To determine if the information contained in the available experimental data is suitable for reliable parameter estimation $\boldsymbol{\Theta}^*$, a practical identifiability analysis (based on concepts of control system theory [43]) was performed on results. This identifiability analysis is based on local sensitivity functions. Such functions quantify the relationship between the outputs and the parameters of the model. It is useful to define the following two nondimensional sensitivity functions:

$$S_{ij} = \frac{\theta_j^*}{\varepsilon_{\max}} \left. \frac{\partial \varepsilon_c(\boldsymbol{\Theta}, t_i)}{\partial \theta_j} \right|_{\theta_j^*} , \tilde{S}_{ij} = \frac{S_{ij}}{\sqrt{\sum_{k=1}^{N} S_{kj}^2}}. \tag{8}$$

The sensitivity ranking of the jth parameter is done through indicators numerically estimated and defined by:

$$\delta_j = \frac{1}{N} \sum_{i=1}^{N} |S_{ij}|. \tag{9}$$

δ_j represents the influence of each parameter in the outputs. Poor identifiability of the model parameters can be due to a small sensitivity of the model results to a parameter, or by a linear approximation dependence of sensitivity functions on the results with respect to the parameters. It is evaluated through a collinearity index which is a measure of the shape of the confidence region:

$$J_B = \sqrt{\frac{1}{\lambda_{\min}}} \tag{10}$$

9

where λ_{min} is the smallest eigenvalue of sensitivity matrix ${}^T\tilde{\boldsymbol{S}}\tilde{\boldsymbol{S}}$. High collinearity index indicates correlation among the parameters. According to Brun et al. [44], parameter subsets with collinearity index smaller than 5 are considered as good and values above 20 are critical.

3. Experimental results

3.1. Aspect and volumic percentage of fibres

[Table 3 about here.]

The characteristics of the produced plates are shown in table 3. V^{p} is the volumic percentage of porosity. The final material has a good aspect. Its appearance is drier than stratified glass/epoxy and stratified carbon/epoxy. Figure 1 shows a cross section of a plate observed by optical microscope. In figure 1(a) we distinguish the UD380 through the thickness of a plate containing eight layers of prepreg. In figure 1(b) we see a yarn coated with resin and we distinguish three neighbouring yarns. In figure 1(c) we distinguish elementary fibres in the middle of that yarn. The lumen is visible although compressed on certain fibres. The cross section of the flax fibre is polygonal. The penetration of the resin within yarns is globally good but not perfect in the middle of yarns (black regions in figure 1(c)). The percentage of fibres V^{r} was calculated by measuring the sizes and the mass of plates and by knowing the density of fibre and matrix (section 2.5). The mean final density ρ^{c} is close to 1.31 and the mean final volumic percentage of porosity is close to $6\,\%$ (see table 3).

[Figure 1 about here.]

3.2. Effect of fibre percentage, yarn titration, and temperature

Figure 2 represents a typical result obtained in tensile tests at room temperature. For a fixed set of parameters, the curves are hardly ever dispersed (fig. 2(a)). This indicates that the fabrication process of the material is reproducible.

[Figure 2 about here.]

On initial examination, this curve has two "linear" regions. The first region makes it possible to measure the apparent longitudinal modulus, E, which is taken as the initial slope. It increases

with the percentage of fibre (fig. 2(b)). Note that variation of strain rate shows that E does not significantly change from $1 \times 10^{-5}\,\mathrm{s}^{-1}$ to $1 \times 10^{-9}\,\mathrm{s}^{-1}$ (fig. 2(c)). Then, the apparent modulus which is mesured at standard speed ($1 \times 10^{-6}\,\mathrm{s}^{-1}$) is very close to the Young's modulus of the material. The limit between the first region and the second region pointed by an arrow in figure 2(a) allows us to introduce a yield point. Considering the narrowness of the first region and the general shape of the curve, we have chosen the point from which the irreversible deformation is equal to $0.02\,\%$. This behaviour – with two regions – was observed for all types of flax/epoxy prepregs. The failure is clean in tension. In this work, we did not witness any "explosion" of the specimen under the action of a collective failure of the fibres. Therefore, the global behaviour of the flax is different from that of carbon fibre or glass fibre [45].

The main results obtained in monotonic tensile test at $20\,^{\circ}\mathrm{C}$ are listed in table 4. σ_u is the ultimate stress, ε_u is the ultimate strain, σ_Y is the yield stress and ε_Y the yield strain.

[Table 4 about here.]

The properties at room temperature are analysed considering, on the one hand, the influence of the fibre percentage of the composite material for the prepreg composed of yarns of $42\,\mathrm{tex}$ (fig. 3), and on the other hand, the influence of the titration of the yarns for the plates made of approximately $60\,\%$ fibre in volume (fig. 4). It is shown that the ultimate stress, the ultimate strain and the apparent longitudinal modulus are proportional to V^{r} (fig. 3(a) and 3(b)) and their evolution versus V^{r} are conform to the rule of mixture [45]. However, for the studied material, as the percentage of porosity is not null, it is important to take it into account when developing the rule of mixture [18]. In a first approach, E, σ_u and ε_u are inversely proportional to the titration (fig. 4(a) and 4(b)), but the relationships must be analysed more closely. It is the result of two trends. On the one hand the fineness of the yarn facilitates the penetration of the resin in the heart of the reinforcement (*i.e.* the yarn). This avoids in the case of fine yarns the impregnation problems that can be seen on larger yarns (fig. 1(c)). On the other hand, with the spinning process, fine yarns are more efficient than larger ones (*i.e.* the worst performing fibres are eliminated at the beginning). This phenomenon is amplified in the case of yarns of $42\,\mathrm{tex}$ by the spinning process used. Wet spinning allows to better separate individual fibres originally linked by pectins, which

increases the area of interface between the resin and the fibres [46]. This results in a nonlinear relationship between the mechanical properties and the titration of the reinforcement (fig. 4(a) and 4(b)). Therefore, using yarns with low titration to decrease the prepreg thickness is a good choice regarding the mechanical properties of composites.

The yield point also depends on titration and on fibre percentage. Yield stress is proportional to V^r and yield strain is inversely proportional to V^r (fig. 3(c)). The increase of the composite performance with V^r causes an overall rotation of the stress/strain curve (fig. 2(b)). Regarding the influence of the titration, there is the same non-linearity as described for other mechanical properties (fig. 4(c)). The yarns of $42\,\mathrm{tex}$ produced by wet spinning is better as reinforcement than yarns of $105\,\mathrm{tex}$ or $400\,\mathrm{tex}$ developed by semi-wet spinning.

[Figure 3 about here.]

[Figure 4 about here.]

The effect of temperature on modulus, failure behaviour, and yield point is exhibited in figure 5. The value of glass transition temperature T_G was measured using a Differential Scanning Calorimetry to be about $143\,°\mathrm{C}$ for epoxy and $100\,°\mathrm{C}$ for FUD180 [47]. Then, the loss of mechanical properties for a temperature above $100\,°\mathrm{C}$ could be correlated to the glass transition temperature of material. Except for the yield point, we show that the results do not really change up to a temperature between $50\,°\mathrm{C}$ and $100\,°\mathrm{C}$. Beyond this threshold temperature, the apparent modulus decreases (fig. 5(a)), and the rupture follows the same trend as previously described: a decrease in the ultimate stress together with an increase in the ultimate strain (fig. 5(b)). However, the first region area continuously decreases with temperature (fig. 5(c)). This decrease can be influenced by reinforcement behaviour, matrix behaviour, and by reinforcement/matrix interface evolution with temperature.

[Figure 5 about here.]

3.3. Focus on the mechanical behaviour

We now focus our analysis on the mechanical behaviour of flax/epoxy composite at $20\,°\mathrm{C}$. Two creep tests on FFRP, one in the first region, and the other in the second region, have confirmed the irreversible character of the second region at room temperature (fig. 6).

12

[Figure 6 about here.]

Figure 7 shows typical results of the tensile test in repetitive progressive loading (RPL) at various temperatures. The monotonic tensile curve at room temperature is included for comparison. We notice that the test at $50\,°\mathrm{C}$ is perfectly fixed on that curve (the same applies to the result at $20\,°\mathrm{C}$, not represented in the figure), meaning that the prepregs are not degraded in tension below $50\,°\mathrm{C}$. We also notice that the first discharge does not present any irreversible strain at $20\,°\mathrm{C}$ or $50\,°\mathrm{C}$ (fig. 7(b)). Therefore, for this material, the yield stress at room temperature is higher than $50\,\mathrm{MPa}$ (instruction of the first loading).

[Figure 7 about here.]

It was observed that the utilised reinforcements are yarns which are twisted. Moreover the FUD shows a slight warp shrinkage. But these two elements can not explain the observation of a yield point because, as mentioned in the introduction, the two regions are observed for FFRP reinforced by both unidirectional fibres and random mat of flax [20, 22].

The most important results obtained in RPL in tensile test are exhibited in table 5. The hysteresis observed during the successive unloading/reloading after the first one means that the material dissipates a considerable amount of energy during these phases.

[Table 5 about here.]

These results led us to model the behaviour of the material by a phenomenological model with kinematic hardening taking viscosity into account.

4. Identification results

4.1. Material constitutive equations

In this section we develop the viscoelastoplastic model presented in section 2.7 in the case of uni-axial behaviour of UD reinforcements at $20\,°\mathrm{C}$. Note that the used methodology would be the same for FUD composites, but the inelastic material parameters would be different (according to the difference of properties given in table 4).

The state variables can be divided into observable variables and internal variables as defined in table 6.

13

Based on experimental results, the free energy and dissipation potential are proposed in the following equations:

$$\psi(\varepsilon^e, \alpha_i) = \frac{1}{2\rho}E(\varepsilon^e)^2 + \frac{1}{2\rho}\sum_{i=1}^{3}C_i\alpha_i^2 \tag{11}$$

$$\Omega = \Omega^{ve} + \Omega^{vp} = \frac{1}{2\eta}(\sigma - X_1)^2 + \frac{1}{2K}\langle f\rangle^2 \tag{12}$$

with

$$f = |\sigma - X_2 - X_3| - \sigma_Y + \frac{\gamma_3}{2C_3}X_3^2 \tag{13}$$

where ρ is the mass density, E and σ_Y are the Young's modulus and the initial yield stress, respectively. η and K are viscosity coefficients corresponding to elastic and plastic phenomena, respectively. C_1 is the viscoelastic stiffness. C_2, C_3 and γ_3 are hardening coefficients. C_2 characterizes linear kinematic hardening. C_3 and γ_3 refer to nonlinear kinematic hardening coupled to a contraction of elastic domain in order to improve the unloading modeling in RPL tests. The symbols $\langle\rangle$ denote Macauley's brackets such as $\langle x\rangle = 0$ if $x < 0$ and $\langle x\rangle = x$ if $x \geq 0$.

The state laws defined by equations (2) and (3) becomes:

$$\sigma = E\varepsilon^e \tag{14}$$

$$X_i = C_i\alpha_i. \tag{15}$$

And the evolution of internal variables defined by equations (4) and (5) becomes:

$$\dot{\varepsilon}^{ve} + \dot{\varepsilon}^{vp} = \frac{1}{\eta}(\sigma - X_1) + \frac{\langle f\rangle}{K}\text{sign}(\sigma - X_2 - X_3) \tag{16}$$

$$\dot{\alpha}_1 = \frac{1}{\eta}(\sigma - X_1) \tag{17}$$

$$\dot{\alpha}_2 = \frac{\langle f\rangle}{K}\text{sign}(\sigma - X_2 - X_3) \tag{18}$$

$$\dot{\alpha}_3 = \frac{\langle f\rangle}{K}\left[\text{sign}(\sigma - X_2 - X_3) - \frac{\gamma_3}{C_3}X_3\right]. \tag{19}$$

From a rheological point of view the model proposed here is, for elastic contribution, a linear spring E, and for viscoelastic contribution, a classical Kelvin-Voigt model which comprises a

14

linear viscous damper η and a linear spring C_1 – with internal stress X_1 – connected in parallel. For viscoplastic contribution, a more complex model is required, it consists in adding two kinematic hardenings such as [48, 49]: a linear kinematic hardening [50], in which the evolution of the kinematic variable X_2 is collinear with the evolution of the plastic strain and a nonlinear kinematic hardening X_3 [51]. In addition, a coupling between translation and contraction during loading of the elastic domain is added through the last term of equation (13). Finally, seven inelastic parameters have to be identified: $\Theta = [\theta_1, \cdots, \theta_7]$. They are summarized in table 7. The Young's modulus was chosen from the measurements on UD composites ($E \simeq 26\,900\,\mathrm{MPa}$, cf. table 4).

[Table 7 about here.]

4.2. Parameters identification

The inverse method approach defined in section 2.8 is used to extract constitutive inelastic parameters of UD composites at $20\,°\mathrm{C}$ from the strain measurements on two tests:

- Test A: Repetitive progressive loading in tension (fig. 7),

- Test B: Creep in tension at $29\,\mathrm{MPa}$ (fig. 6).

The result of the identification is presented in table 7. Figure 8 shows simulated responses with identified parameters for RPL and creep tests. The experimental data are respectively the RPL data at $20\,°\mathrm{C}$ and the creep data at $29\,\mathrm{MPa}$ presented in figure 6.

[Figure 8 about here.]

The very low value of the K parameter ($< 10^{-3}\eta$) should be noted; this indicates that viscoplastic phenomena are about 1000 time faster than viscoelastic ones. Figure 9 illustrates the elastic, viscoelastic and viscoplastic contributions for RPL and creep test at $20\,°\mathrm{C}$. It is clear that at room temperature, the RPL test at usual strain rate activates mainly viscoplastic phenomena and the creep test – here under the initial yield stress – activates mainly viscoelastic phenomena.

[Figure 9 about here.]

15

4.3. Identifiability analysis and model validation

To ensure parameter identification, sensitivity analysis was applied through δ_i indicators defined by equation (9). Figure 10(a) shows these indicators as numerically estimated. As can be seen, the influence on the outputs of each parameter is of the same magnitude (prerequisite for reliable identifiability).

A test of non collinearity of the sensibility matrix has been conducted in order to confirm that all parameters are identifiable. The collinearity index $J_B = 7.7$, calculated using equation (10), indicates an acceptable identifiability level ($J_B < 10$). Figure 10(b) shows the change of J_B with the number of data points included in the calculation. The evolution of J_B illustrates the complementarity of RPL and creep tests in the identification strategy. Combination of both tests allows us to achieve the threshold ($J_B < 20$).

[Figure 10 about here.]

Two validation tests were finally done on a creep test at $126\,\mathrm{MPa}$ (fig. 11(a)) and a relaxation test at $0.33\,\%$ (fig. 11(b)). The experimental data are respectively the creep test data at $126\,\mathrm{MPa}$ used in figure 6 and relaxation test data not presented before. It should be noted that these two tests are complementary with the tests used for identification (fig.8). Figure 11 shows the fit between simulation and experimental data, which validates our model identification.

[Figure 11 about here.]

5. Discussion

The correlation between experimental results and simulation is good for a model with only seven parameters. At room temperature, the proposed model allows us to correctly simulate the behaviour of flax/epoxy UD in repetitive progressive loading, creep test and relaxation test. The used parameters take into account viscoelastic and viscoplastic contributions. The first region of tensile curves is quasi-elastic and the second region is viscoelastoplastic. It appears that the viscoelastic contribution is negligible on the RPL behaviour (see fig. 9 and fig. 10). Note that in such a case the apparent longitudinal modulus measured in the first region is very close to the Young's modulus of the material, as shown in section 3.2. The hysteresis loops observed in

repetitive progressive loading come from a kinematic hardening coupled to a contraction of the elastic domain.

The possibility of an interface fibrer-matrix mechanism was envisaged, but the two regions are observed on FFRP by polypropylene matrix [22] or after severe hygrothermal ageing [52] as by flax/paper/epoxy composites [21]. There is no reason why the interface should be similar for all these studies, therefore we excluded the fact that yield point of FFRP originates from an interface fibre-matrix mechanism. Furthermore, we have checked that the resin does not show a yield point at room temperature as in the case of the composite. Therefore the yield point of FFRP arises from flax reinforcement.

In the case of the tested materials, the reinforcement is multiscale. The bigger scales are that of fabric and that of unidirectionnal yarn. The median scales are that of bundle of fibres and that of individual fibre itself. The lower scale of reinforcement is that of microfibril which is the main component of individual fibre. In tensile test, flax yarn does not show any threshold [18] but flax fibres show a decrease of the apparent modulus after $\varepsilon \simeq 0.2\%$ and an increase at the end of stress-strain curve [53, 54, 55]. The major explanation of this behaviour is the cellulose microfibrils reorientation [53]. The fact that FFRP has a yield point at $\varepsilon \simeq 0.2\%$ coupled to a contraction of elastic domain with deformation and with temperature tends to prove a correlation between these phenomena and the behaviour of individual flax fibres.

We are finally led to the conclusion that mechanical behaviour of unidirectionnel flax/epoxy composite is mainly due to the individual flax fibre beaviour. The end of the first region of the monotonic tensile test occurs on average at $\varepsilon = 0.2\%$, value which hardly depends on fibre volume fraction (fig. 3(c)), titration (fig. 4(c)), temperature (fig. 5(c)) and moisture rate of the composite [52]. It could be correlated to the beginning of a collective reorientation of microfibrils. The relationship between microfibrilar angle and Young's modulus of individual flax fibres was recently demonstrated with X-ray diffraction on a bundle of fibres that were not embedded into a polymer matrix [56]. The measurement of the reorientation of microfibrils during a tensile test by the same method is an exciting challenge to take up but it not seems possible with the tested material due to the complexity of the reinforcement.

6. Conclusion

Four types of laminate composites were elaborated and tested from two categories of prepregs intended for an unidirectional reinforcement. The prepregs were produced industrially from linen yarns. The four prepregs contain yarns of 400, 105 or $42\,\mathrm{tex}$. Our results show that the failure stress, the failure strain and the apparent longitudinal modulus are proportional to the percentage of fibres and are inversely proportional to the titration of yarns. The finest linen threads mostly used in the textile industry have a titration of $28\,\mathrm{tex}$ or exceptionally $21\,\mathrm{tex}$. Although the technological difficulty to make such yarns is enormous, their use for the development of reinforcement is then a promising path to be explored.

In comparison with conventional composites, the flax fibre reinforced polymers (FFRP) show two remarkable behaviours which have hardly been studied in the literature until now. The first is a yield point beyond which there are irreversible strains. This is demonstrated by creep tests. The second is a viscous behaviour whatever the temperature. This is demonstrated using repeated progressive loadings and monotonic tensile tests at different strain rates. In order to analyze these two behaviours, a combined viscoelastic-viscoplastic model coupling a standard linear solid (SLS) model and a viscoplastic model with nonlinear kinematic hardening is developed. An inverse method is used to extract the constitutive parameters from the experimental strain measurements and a practical identifiability analysis lead to justify the ability to identify the "true" parameters values from only two tests (RPL and creep). We show that the viscoelastic contributions are negligible at normal condition, however they do explain creep and relaxation behaviour. The main explanation for the overall behaviour of flax/epoxy comes from the plastic deformation of the reinforcement after a short quasi-elastic region. This leads to a non-linear kinematic hardening of the composite material coupled to a contraction of the elastic domain.

Besides their interest in terms of density and environmental promises, FFRP will plasticize after a short elastic behaviour. This offers highly promising prospects regarding this category of composite materials. A set of specific tests and simulations on unidirectionnal FFRP (without twisted yarns), under a wide range of temperature and strain rate is expected to confirm our hypothesis and to make more general description of FFRP viscoelastoplastic behaviour. Particu-

larly, it seems possible to measure the reorientation of cellulose microfibrils with deformation with X-ray diffraction.

Acknowledgement

References

[1] A. K. Mohanty, M. Misra, L. T. Drzal, Sustainable bio-composites from renewable resources: Opportunities and challenges in the green materials world, J Polym Environ 10 (2002) 19–26.

[2] N. Tucker, M. Jonhson, Low Environmental Impact Polymers, Rapra Technology Limited, Shrewsbury, 2004.

[3] D. Nabi Saheb, J. P. Jog, Natural fiber polymer composites, Adv Polym Tech 18 (1999) 351–363.

[4] G. Bogoeva-Gaceva, M. Avella, M. Malinconico, A. Bužarovska, A. Grozdanov, G. Gentile, M. E. Errico, Natural fiber eco-composites, Polym Composite 28 (2007) 98–107.

[5] R. F. Gibson, A review of recent research on mechanics of multifunctional composite materials and structures, Compos Struct 92 (2010) 2793–2810.

[6] T. Huber, J. Müssig, O. Curnow, S. Pang, S. Bickerton, M. P. Staiger, A critical review of all-cellulose composites, J Mater Sci 47 (2012) 1171–1186.

[7] R. W. Kessler, U. Becker, R. Kohler, B. Goth, Steam explosion of flax – a superior technique for upgrading fibre value, Biomass Bioenerg 14 (1998) 237–249.

[8] S. V. Joshi, L. T. Drzal, A. K. Mohanty, S. Arora, Are natural fiber composites environmentally superior to glass fiber reinforced composites, Compos Part A-Appl S 35 (2004) 371–376.

[9] M. Assarar, D. Scida, A. El Mahi, C. Poilâne, R. Ayad, Influence of water ageing on mechanical properties and damage events of two reinforced composite materials: flax-fibres and glass-fibres, Mater Design 32 (2011) 788–795.

[10] S. Liang, P. B. Gning, L. Guillaumat, A comparative study of fatigue behaviour of flax/epoxy and glass/epoxy composites, Compos Sci Technol 72 (2012) 535–543.

[11] A. K. Bledzki, J. Gassan, Composites reinforced with cellulose based fibres, Prog Polym Sci 24 (1999) 221–274.

[12] P. Wambua, I. Verpoest, J. Ivens, Natural fibres: can they replace glass in fibre reinforced plastics?, Compos Sci Technol 63 (2003) 1259–1264.

[13] J. Summerscales, N. P. J. Dissanayake, A. S. Virk, W. Hall, A review of bast fibres and their composites. Part 1 – fibres as reinforcements, Compos Part A-Appl S 41 (2010) 1329–1335.

[14] K. Charlet, J.-P. Jernot, J. Bréard, M. Gomina, Scattering of morphological and mechanical properties of flax fibres, Ind Crop Prod 32 (2010) 220–224.

[15] K. Van de Velde, P. Kiekens, Effect of material and process parameters on the mechanical properties of unidirectional and multidirectional flax/polypropylene composites, Compos Struct 62 (2003) 443–448.

[16] X. Li, L. G. Tabil, S. Panigrahi, Chemical treatments of natural fiber for use in natural fiber-reinforced composites: a review, J Polym Environ 15 (2007) 25–33.

[17] S. Kalia, B. S. Kaith, I. Kaur, Pretreatments of natural fibers and their application as reinforcing material in polymer Composites—A review, Polym Eng Sci (2009) 1253–1272.

[18] Z. E. Cherif, C. Poilâne, T. Falher, A. Vivet, N. Ouail, B. Ben Doudou, J. Chen, Influence of textile treatment on mechanical and sorption properties of flax/epoxy composites, Polym Composite 34 (2013) 1761–1773.

[19] S. Goutianos, T. Peijs, B. Nystrom, M. Skrifvars, Development of flax fibre based textile reinforcements for composite applications, Appl Compos Mater 13 (2006) 199–215.

[20] K. Oksman, High quality flax fibre composites manufactured by the resin transfer moulding process, J Reinf Plast Comp 20 (2001) 621–627.

[21] G. Lebrun, A. Couture, L. Laperrière, Tensile and impregnation behavior of unidirectional hemp/paper/epoxy and flax/paper/epoxy composites, Compos Struc 103 (2013) 151–160.

[22] H. L. Bos, J. Müssig, M. J. A. Van den Oever, Mechanical properties of short-flax-fibre reinforced compounds, Compos Part A-Appl S 37 (2006) 1591–1604.

[23] S. Ben Brahim, R. Ben Cheikh, Influence of fibre orientation and volume fraction on the tensile properties of unidirectional alfa-polyester composite, Compos Sci Technol 67 (2007) 140–147.

[24] N. Suizu, T. Uno, K. Goda, J. Ohgi, Tensile and impact properties of fully green composites reinforced with mercerized ramie fibers, J Mater Sci 44 (2009) 2477–2482.

[25] J. Lemaitre, J. L. Chaboche, Mechanics of solid materials, Cambridge University Press, Cambridge, 1994.

[26] F. Thiébaud, D. Perreux, Overall mechanical behaviour modelling of composite laminate, Eur J Mech A-Solids 15 (1996) 423–445.

[27] K. Charlet, C. Baley, C. Morvan, J.-P. Jernot, M. Gomina, J. Bréard, Characteristics of hermès flax fibres as a function of their location in the stem and properties of the derived unidirectional composites, Compos Part A-Appl S 38 (2007) 1912–1921.

[28] K. Charlet, C. Baley, C. Morvan, J.-P. Jernot, M. Gomina, J. Bréard, Influence of an agatha flax fibre location in a stem on its mechanical, chemical and morphological properties, Compos Part A-Appl S (2009) 1399–1403.

[29] I. Van de Weyenberg, J. Ivens, A. De Coster, B. Kino, E. Baetens, I. Verpoest, Influence of processing and chemical treatment of flax fibres on their composites, Compos Sci Technol 63 (2003) 1241–1246.

[30] L. Y. Mwaikambo, Review of the history, properties and application of plant fibres, Afr J Sci Technol 7 (2006) 120–133.

[31] H. Bos, M. J. A. Van den Œver, O. C. J. J. Peters, Tensile and compressive properties of flax fibres for natural fibre reinforced composites, J Mater Sci 37 (2002) 1683–1692.

[32] B. P. Saville, Physical testing of textiles, Woodhead Publishing Limited, Cambridge, 1999.

[33] J. Van Raemdonck, inventor, march 8th 2007. Method for preparing thermosetting or thermoplastic polymer or elastomer composites that are reinforced with natural fibers, and their multiple applications as construction material. Patent WO/2007/025782.

[34] http://www.lineo.eu/. Accessed June 25, 2013.

[35] http://www.huntsman.com/. Accessed June 25, 2013.

[36] International Organization for Standardization, Plastics – Determination of tensile properties – Part 4: Test conditions for isotropic and orthotropic fibre-reinforced plastic composites, International Standard ISO 527-4:1997.

[37] International Organization for Standardization, Plastiques – Plastics – Determination of tensile properties – Part 5: Test conditions for unidirectional fibre-reinforced plastic composites, International Standard ISO 527-5:2009.

[38] International Organization for Standardization, Plastics – Methods for determining the density of non-cellular plastics – Part 1: Immersion method, liquid pyknometer method and titration method, International Standard ISO 1183-1:2012.

[39] R. Mansecal, Cellulose, in: Polymer Data Handbook, J. E. Mark Edt., Oxford University Press, Oxford, 1999.

[40] S. K. Batra, Other long vegetable fibers: abaca, banana, sisal, henequen, flax, ramie, hemp, sunn, and coir, in: Handbook of Fiber Chemistry, third edition Edition, Vol. 16 of International Fiber Science and Technology, Lewin M, 2007, pp. 453–520.

[41] B. Halphen, Q. S. Nguyen, Sur les matériaux standards généralisés, J. de Mécanique, 14 (1975), 39–63.

[42] F. Richard, MIC2M, modélisation et identification du comportement mécanique non linéaire des matériaux (1999). URL http://mic2m.univ-fcomte.fr. Accessed July 10, 2013.

[43] D. Dochain, P. Vanrolleghem, Dynamical modelling and estimation in wastewater treatment processes, IWA Publishing, London, 2001.

[44] R. Brun, P. Reichert, H.R. Künsch, Practical identifiability analysis of large environmental simulation models, Water Resources Research 37 (2001) 1015–1030.

[45] J.-M. Berthelot, Composite Materials: Mechanical Behavior and Structural Analysis, Springer-Verlag, New-York, 1999.

[46] Z. E. Cherif, C. Poilâne, L. Momayez, J. Chen, Optimisation d'un pré-imprégné lin/époxy industriel, Revue des Composites et Matériaux Avancés 21 (2011) 119–128, in Comportement mécanique des renforts et des composites tissés, JST AMAC, Orléans, Mai 26-27, 2010.

[47] M. Karray, Caractérisation des propriétés mécanique et électrique des matériaux composites par méthode holo-

graphique numérique 3D et analyse diélectrique, PhD Thesis, Université du Maine, France, (2012).

[48] J.-L. Chaboche, G. Rousselier, On the plastic and viscoplastic constitutive-equations. 1. Rules developed with internal variable concept, J Press Vess-T ASME 105 (2) (1983) 153–158.

[49] J.-L. Chaboche, G. Rousselier, On the plastic and viscoplastic constitutive-equations. 2. Application of internal variable concepts to the 316 stainless-steel, J Press Vess-T ASME 105 (2) (1983) 159–164.

[50] W. Prager, Recent developments in the mathematical theory of plasticity, J Appl Phys 20 (3) (1949) 235–241.

[51] P. J. Armstrong, C. O. Frederick, A mathematical representation of the multiaxial bauschinger effect, Tech. Rep. RD/B/N731, Central Electricity Generating Board and Berkeley Nuclear Laboratories, Research & Development Department (1966).

[52] D. Scida, M. Assarar, C. Poilâne, R. Ayad, Influence of hygrothermal ageing on the damage mechanisms of flax-fibre reinforced epoxy composite, Compos Part B-Eng 48 (2013) 51–58.

[53] C. Baley, Analysis of the flax fibres tensile behaviour and analysis of the tensile stiffness increase, Compos Part A-Appl S 33 (2002) 939–948.

[54] A. Nechwatal, K.-P. Mieck, T. Reußmann, Developments in the characterization of natural fibre properties and in the use of natural fibres for composites, Compos Sci Technol 63 (2003) 1273–1279.

[55] T. Nilsson, P. J. Gustafsson, Influence of dislocations and plasticity on the tensile behaviour of flax and hemp fibres, Compos Part A-Appl S 38 (2007) 1723–1728.

[56] A. Bourmaud, C. Morvan, A. Bouali, V. Placet, P. Perré, C. Baley, Relationships between micro-fibrillar angle, mechanical properties and biochemical composition of flax fibers, Ind Crops Prod 44,(2013) 343–351.
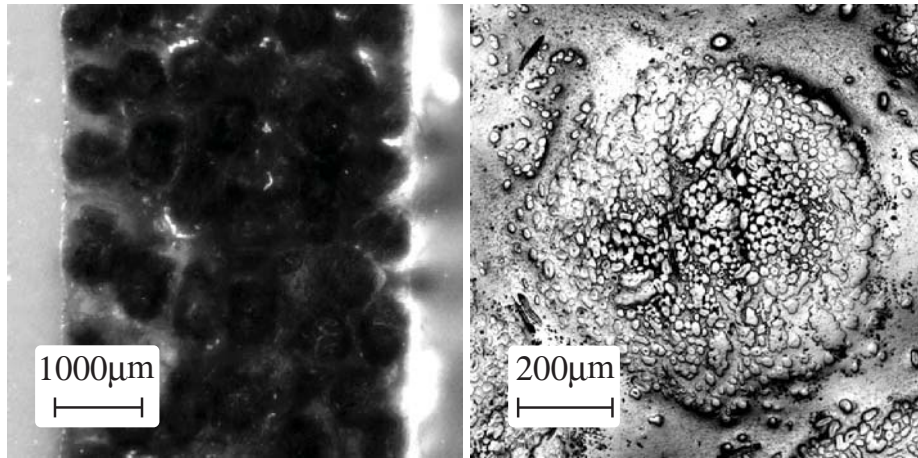
(a) transverse section of a sample (b) one yarn
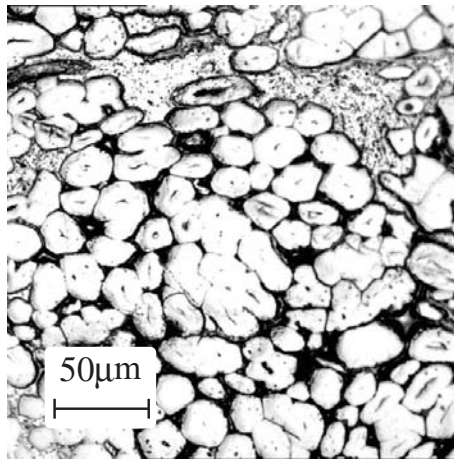
(c) several fibres in the middle of a yarn

Figure 1: Optical views of a cross section of a plate (UD380, 8 layers)
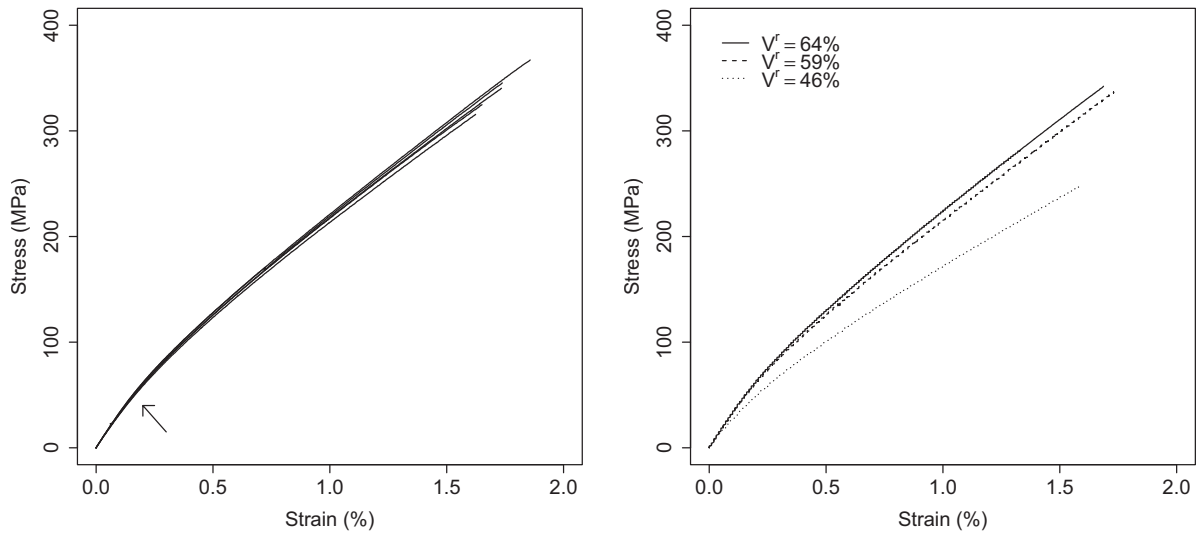
(a) reproducibility of typical test (five specimens, strain rate $10^{-6}\,\mathrm{s}^{-1}$)

(b) evolution with volumic percentage of fibre, strain rate $10^{-6}\,\mathrm{s}^{-1}$)
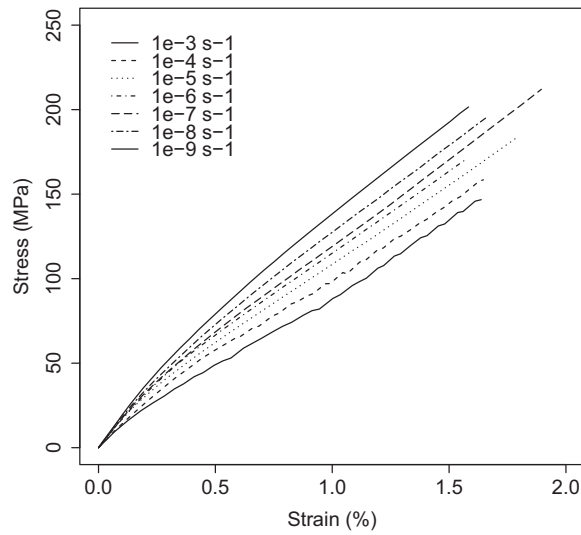
(c) evolution with strain rate

Figure 2: Typical stress-strain curves obtained in tensile test at room temperature, the arrow points the transition from the first to the second region (FUD180)
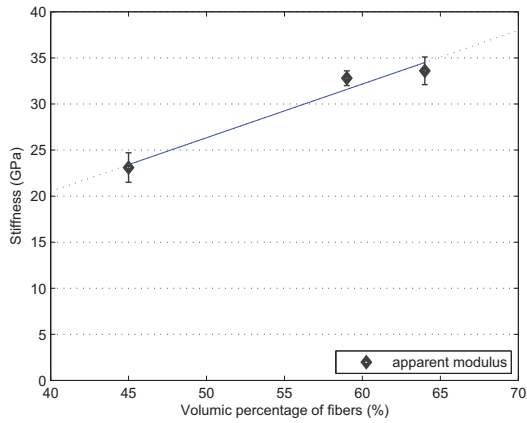
(a) apparent modulus
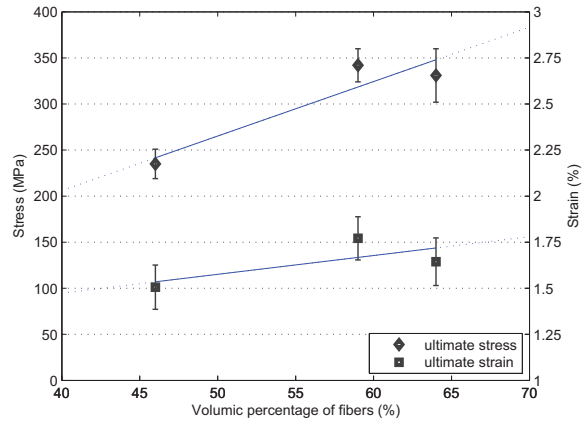
(b) stress and strain at failure
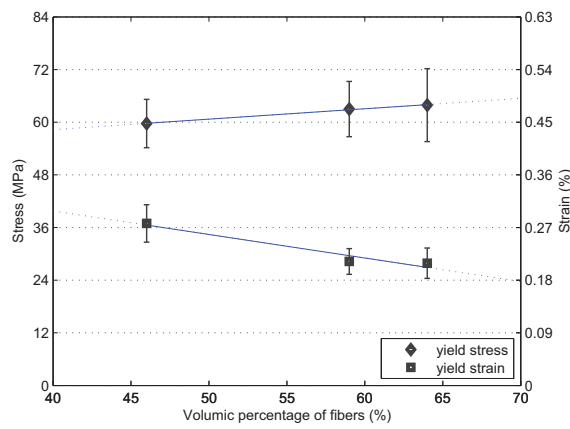
(c) yield point

Figure 3: Effect of percentage of fibres, prepreg composed of yarns of $42\,\mathrm{tex}$ (5 specimens at 45%, 13 specimens at 60%, 5 specimens at 65%, strain rate $10^{-6}\,\mathrm{s}^{-1}$)
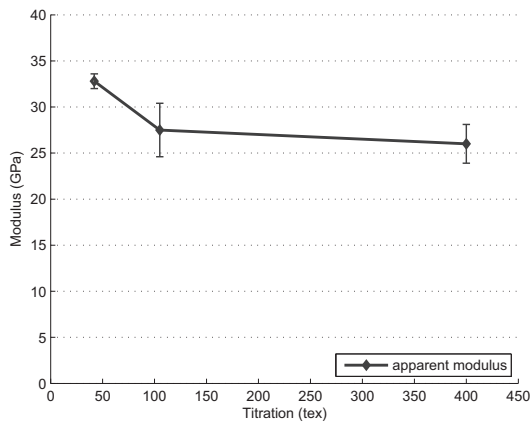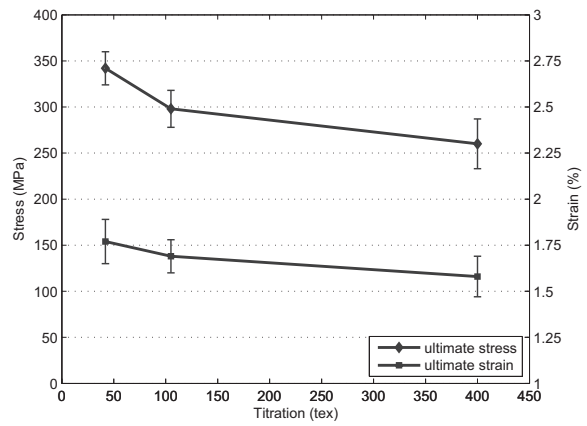
(a) apparent modulus

(b) stress and strain at failure
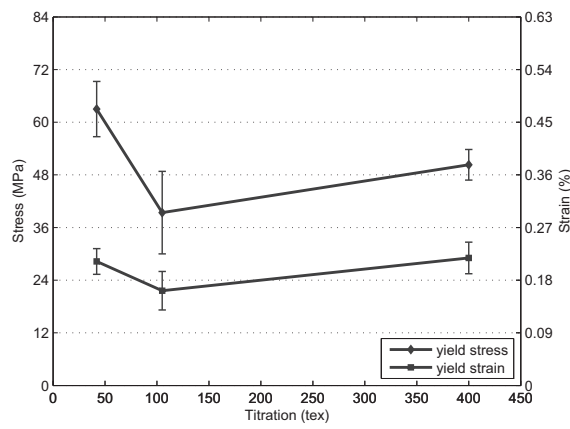
(c) yield point

Figure 4: Effect of titration of yarns, laminates with $60\,\%$ in volume of fibres (13 specimens at $42\,\mathrm{tex}$, 4 specimens at $105\,\mathrm{tex}$, 5 specimens at $400\,\mathrm{tex}$, strain rate $10^{-6}\,\mathrm{s}^{-1}$)
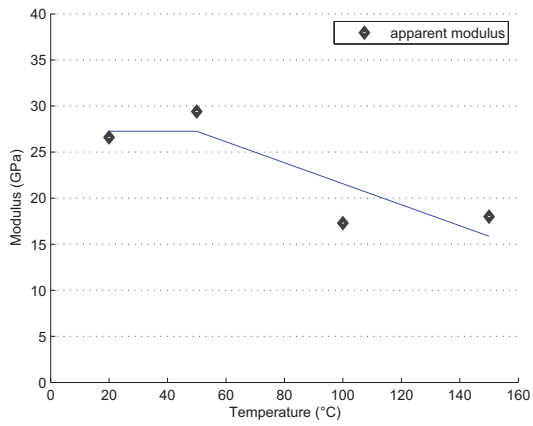
(a) apparent modulus
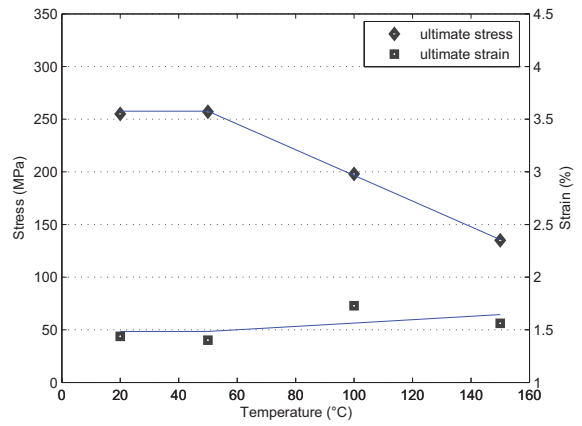
(b) stress and strain at failure
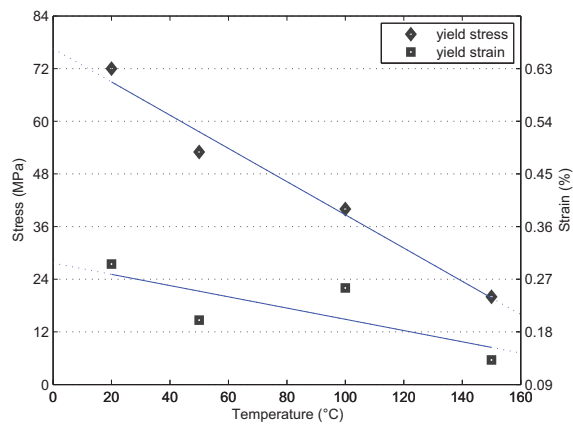
(c) yield point

Figure 5: Effect of temperature (UD380, 1 specimen by point, strain rate $10^{-6}\,\mathrm{s}^{-1}$)
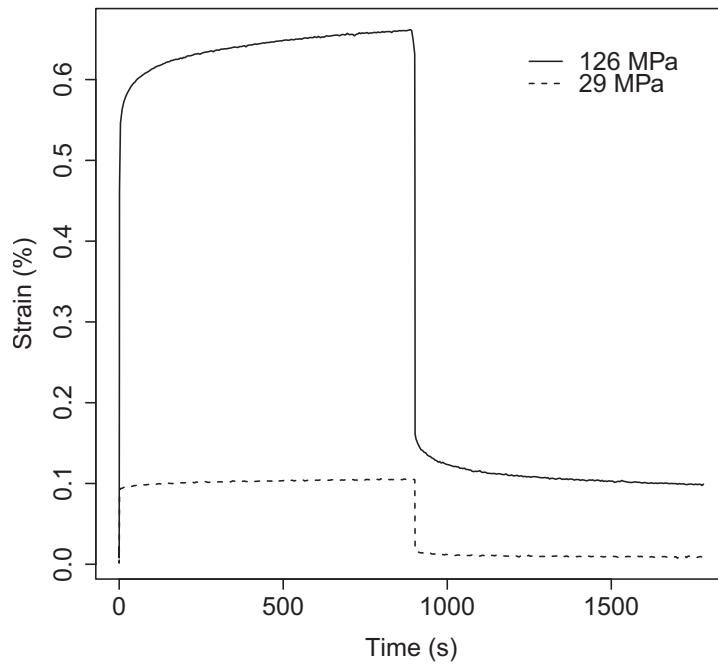
Figure 6: Two creep tests, one at $29\,\mathrm{MPa}$ in the first region, one at $126\,\mathrm{MPa}$ in the second region (UD200)
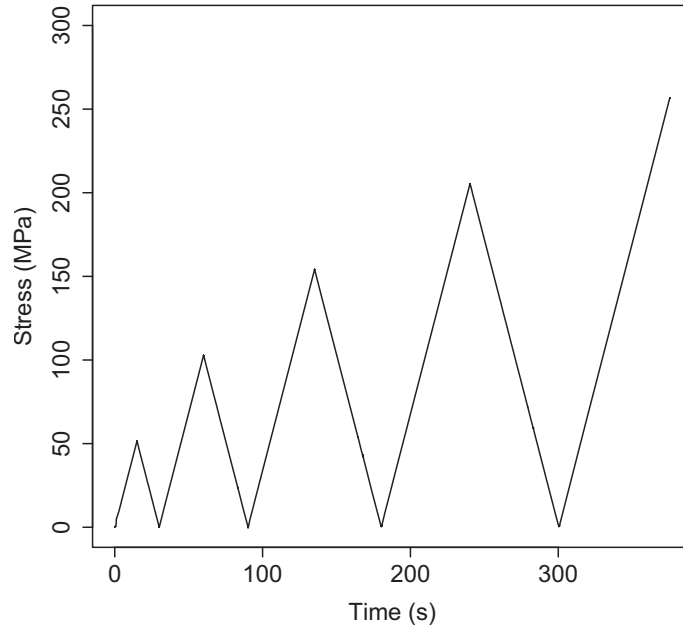
(a) instruction
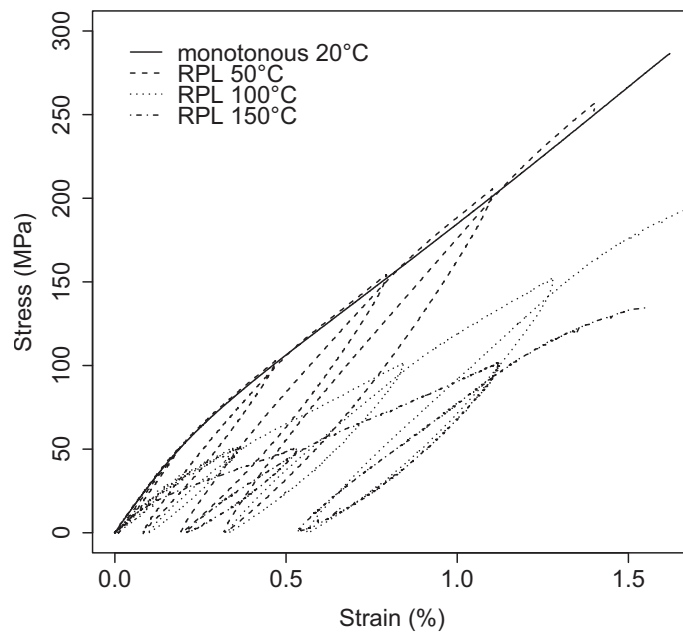
(b) result according to temperature (UD380)

Figure 7: Repetitive progressive loading in tension (RPL at 20 °C not include)

29
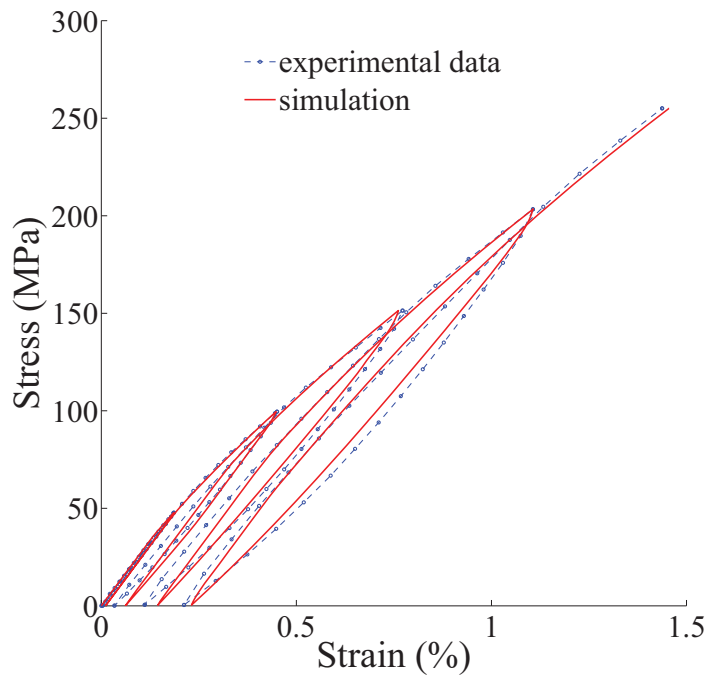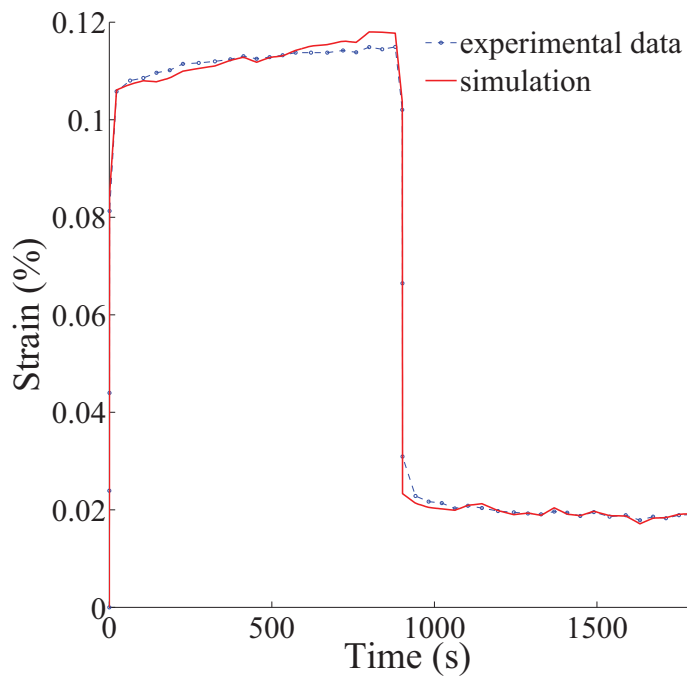
(a) RPL (UD380)

(b) creep test at 29 MPa (UD200)

Figure 8: Simulation response vs experimental data for repetitive progressive loading and creep test at 20 °C

30
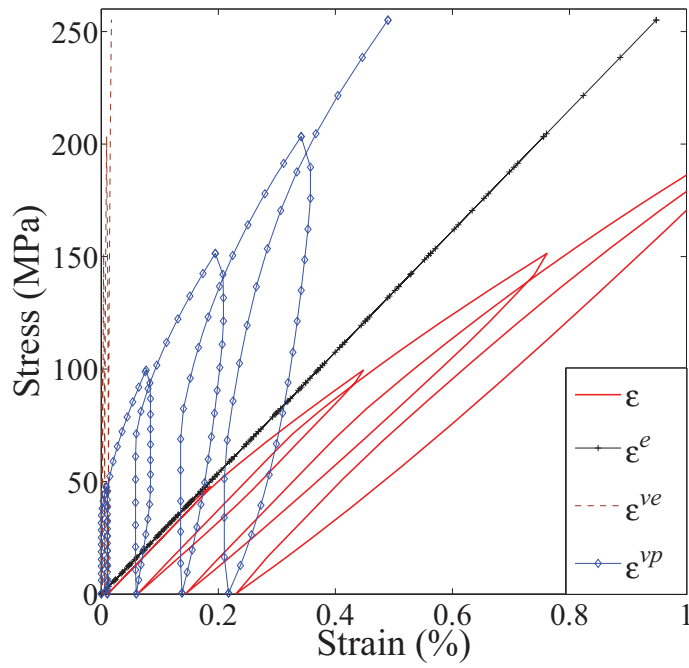
(a) RPL (UD380)
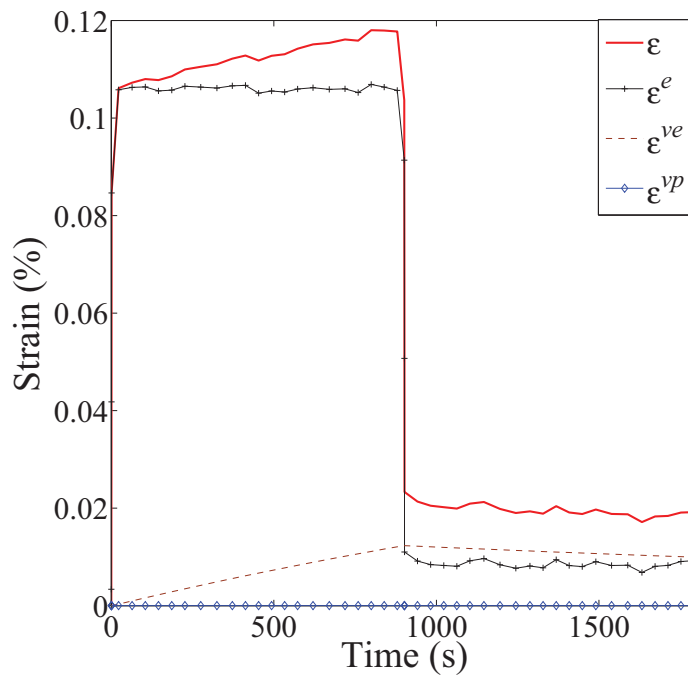
(b) creep test at 29 MPa (UD200)

Figure 9: Simulation response according to elastic contribution, viscoelatic contribution and viscoplastic contribution for RPL and creep test at 20 °C
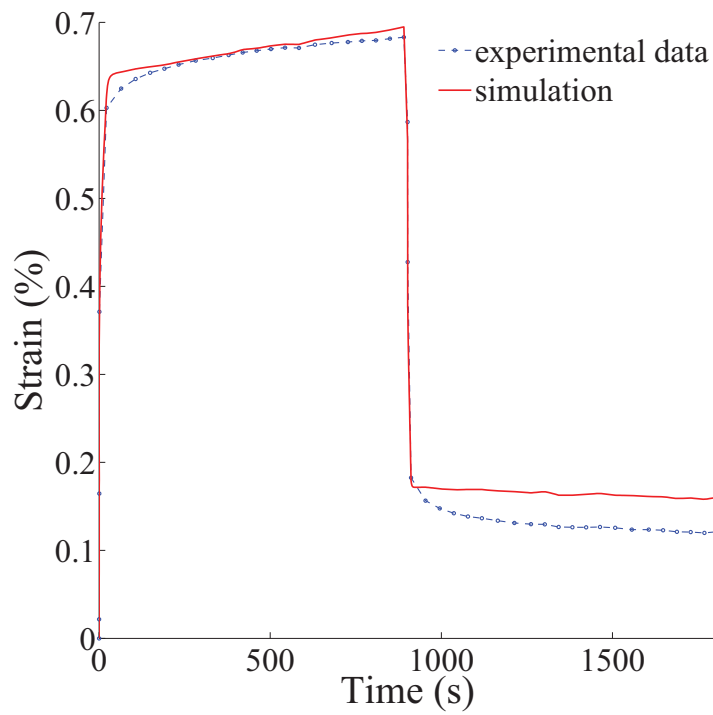
31
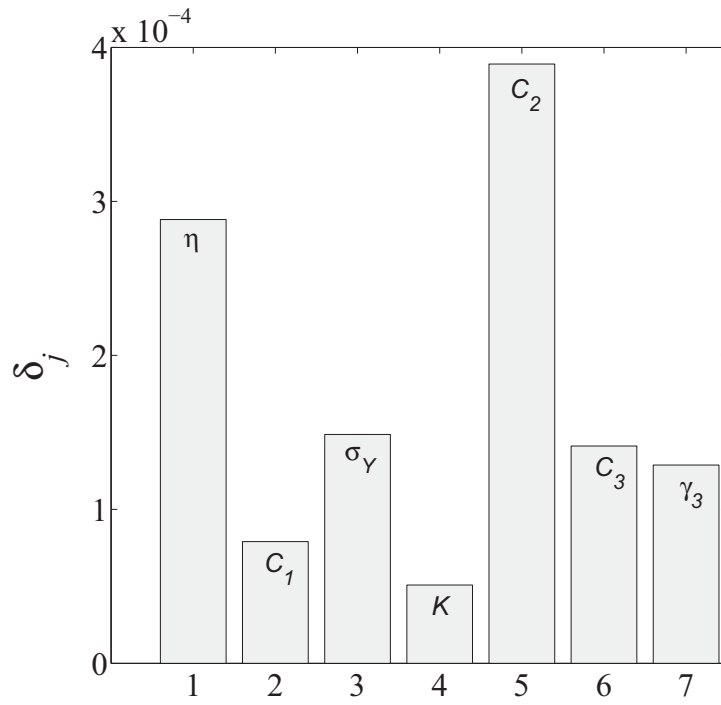
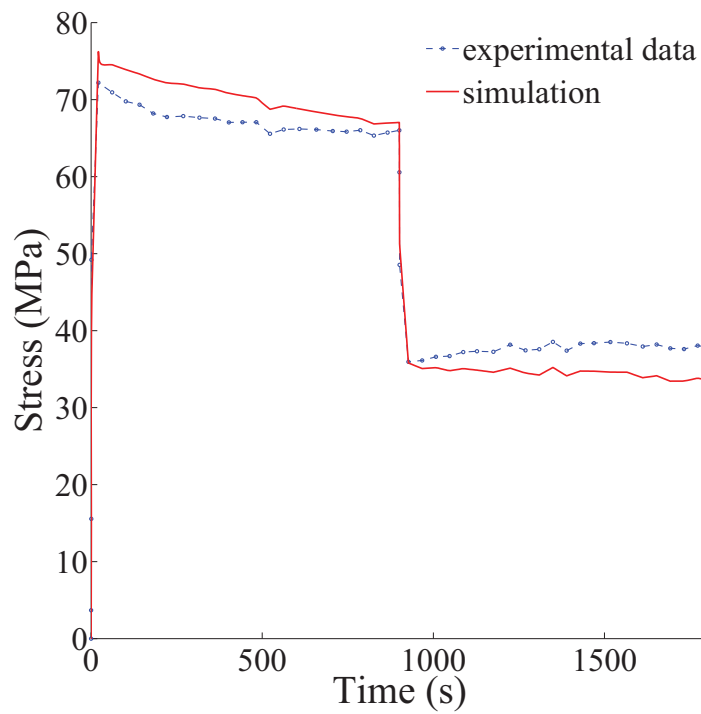(a) sensibility indicators δ_j
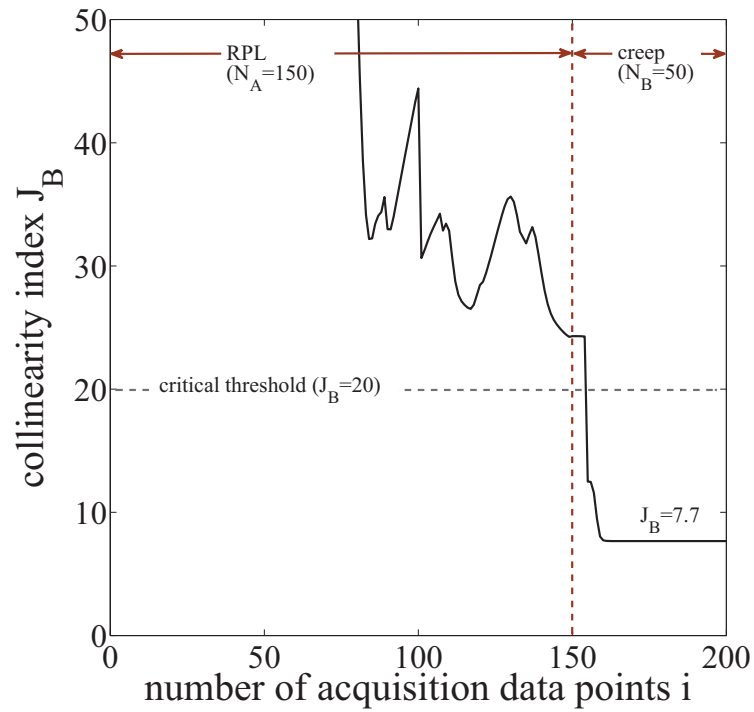
(b) collinarity index J_B

Figure 10: Identifiability analysis results estimated by equations (9) and (10)

(a) creep test at 126 MPa (UD200)

(b) relaxation at 0.33% (UD200)

Figure 11: Validation of the model on creep test and relaxation test at 20°C

33

List of Tables

Table 1: Mechanical properties of flax and conventional fibres

Property	Flax	E-Glass	Aramid	Carbon
ρ (kg dm^{-3})	1.54	2.54	1.45	1.94
E (GPa)	58	72	135	588
σ_u (MPa)	800	2220	3000	3920
ε_u (%)	3.3	3	4.5	0.7
E/ρ (GPa dm^3 kg^{-1})	38	28	93	303
σ_u/ρ (MPa dm^3 kg^{-1})	520	875	2700	2020

Table 2: Characteristics of experimented prepregs
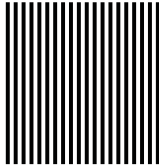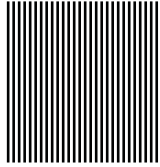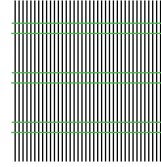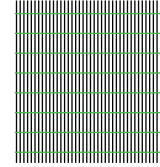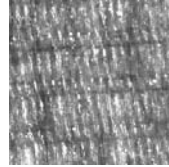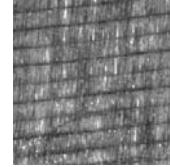
	UD380	UD200	FUD180	FUD115
Titration of yarn (tex)	400	105	42	42
Weight of fabric (g m^{-2})	400	223	180	115
Weft/warp ratio	0	0	1/19	1/8
Model of the texture				
Aspect				

Table 3: Main characteristics of the tested specimens at $2\,\mathrm{mm\,min^{-1}}$ (RPL: repeated progressive loading)

Material	Number of specimens	folds	Instruction	Thickness (mm)	$V^{\mathrm{r}}(\%)$	$V^{\mathrm{p}}(\%)$	ρ^{c} $(\mathrm{kg\,dm^{-3}})$
UD380	5	8	monotonous	3.8	57	6	1.31
	4	6	RPL	2.8	59	5	1.31
UD200	4	8	monotonous	2.2	60	13	1.22
FUD180	4	10	monotonous	2	60	8	1.36
	5	10	monotonous	2	59	3	1.37
	5	12	monotonous	2.3	64	2	1.33
	4	10	monotonous	2.1	60	6	1.33
FUD115	5	10	monotonous	1.8	46	5	1.24

Table 4: Main results obtained in monotonic tensile test at $20\,\mathrm{°C}$, 4 or 5 specimens per line

Material	V^{r} (%)	E (GPa)		σ_u (MPa)		ε_u (%)		σ_Y (MPa)		ε_Y (%)	
		mean	std	mean	std	mean	std	mean	std	mean	std
UD380	57	26.3	2.1	260	27	1.58	0.11	50.3	3.5	0.22	0.03
UD200	60	27.5	2.9	298	20	1.69	0.09	39.4	9.4	0.16	0.03
FUD180	60	33.1	0.4	357	13	1.93	0.10	59.6	6.6	0.20	0.02
	59	33.3	0.5	339	18	1.72	0.08	61.2	2.4	0.20	0.01
	64	33.6	1.5	331	29	1.64	0.13	63.9	8.3	0.21	0.03
	60	31.8	0.6	330	6	1.72	0.02	68.5	5.8	0.24	0.02
FUD115	46	23.1	1.4	235	16	1.51	0.12	59.7	5.5	0.28	0.03

Table 5: Main results obtained in RPL in tensile test at $20\,\mathrm{°C}$, $50\,\mathrm{°C}$, $100\,\mathrm{°C}$ and $150\,\mathrm{°C}$ (UD380, $V^{\mathrm{r}} = 59\,\%$)

θ (°C)	E (GPa)	σ_u (MPa)	ε_u (%)	σ_Y (MPa)	ε_Y (%)
20	26.6	255	1.44	72	0.30
50	29.4	257	1.40	53	0.20
100	17.3	198	1.73	40	0.25
150	18.0	135	1.56	20	0.13

Table 6: Thermodynamic variables

State variable		Associated variable
observable	internal	
ε		σ (Cauchy stress)
	ε^e	σ
	ε^{in}	$-\sigma$
	α_i	X_i

Table 7: Inelastic material parameters θ_i^*

i	Parameter		θ_i^*
1	η (MPa $\cdot$ s)	viscosity coefficient in elastic domain	1.78×10^8
2	C_1 (MPa)	viscoelastic stiffness	$63\,000$
3	σ_Y (MPa)	initial yield stress	33.2
4	K (MPa $\cdot$ s)	viscosity coefficient in plastic domain	2.24×10^5
5	C_2 (MPa)	kinematic hardening coefficient	$68\,500$
6	C_3 (MPa)	non linear hardening	$33\,900$
7	γ_3	non linear hardening (recall)	964